energies

MDPI

Article

Calorimetric Evaluation of Thermal Stability of Organic Liquid Hydrogen Storage Materials and Metal Oxide Additives

Lin-Jie Xie [1], Jun-Cheng Jiang [1,*], An-Chi Huang [1,*], Yan Tang [1,*], Ye-Cheng Liu [2], Hai-Lin Zhou [2] and Zhi-Xiang Xing [1,*]

[1] School of Environmental and Safety Engineering, Changzhou University, Changzhou 213164, China; 20083700033@smail.cczu.edu.cn

[2] School of Materials Science and Engineering, Changzhou University, Changzhou 213164, China; b20080526@smail.cczu.edu.cn (Y.-C.L.); 19083700424@smail.cczu.edu.cn (H.-L.Z.)

* Correspondence: jiangjc@cczu.edu.cn (J.-C.J.); huangac@cczu.edu.cn (A.-C.H.); tycd@cczu.edu.cn (Y.T.); xingzhixiang@cczu.edu.cn (Z.-X.X.)

Abstract: The effects of two different metal oxide catalysts, SnO and Li_2O, on the dehydrogenation temperature of Carbazole and N-Ethylcarbazole (NE), respectively, were investigated by the Thermogravimetric analyzer and Differential Scanning Calorimetry. Thermogravimetric experiments were performed with 10wt% SnO and Li_2O added to Carbazole and N-Ethylcarbazole, respectively, and compared to pure Carbazole and N-Ethylcarbazole. The results showed that the dehydrogenation temperature of N-Ethylcarbazole was lower than that of Carbazole, and the dehydrogenation temperature of N-Ethylcarbazole +SnO was the lowest, and SnO is an ideal dehydrogenation catalyst for N-Ethylcarbazole. Experiments using Differential Scanning Calorimetry and a Thermogravimetric analyzer showed that with the addition of catalyst, the activation energy of the mixture was more significant and stable, and the thermal hazard was reduced, whereas the relative dehydrogenation temperature was increased. This study provides important information for improving the design of dehydrogenation catalysts for organic liquid hydrogen storage processes.

Keywords: organic liquid hydrogen storage; thermal decomposition; metal oxide catalyst; N-Ethylcarbazole

Citation: Xie, L.-J.; Jiang, J.-C.; Huang, A.-C.; Tang, Y.; Liu, Y.-C.; Zhou, H.-L.; Xing, Z.-X. Calorimetric Evaluation of Thermal Stability of Organic Liquid Hydrogen Storage Materials and Metal Oxide Additives. *Energies* **2022**, *15*, 2236. https://doi.org/10.3390/en15062236

Academic Editor: Eugenio Meloni

Received: 31 January 2022
Accepted: 14 March 2022
Published: 18 March 2022

1. Introduction

As clean energy with excellent development potential in the 21st century, hydrogen has broad application prospects in energy, transportation, industry, and construction. Moreover, because its product is only water and achieves zero CO_2 emissions, hydrogen research has become a key focus across the world [1].

Like the traditional energy sources of natural gas, liquefied petroleum gas, and gasoline, hydrogen has high energy and high deflagration hazard [2].

In the past, faulty hydrogen storage practices have resulted in far too many hydrogen explosion mishaps worldwide. Two people were killed and six others were injured when a hydrogen fuel storage tank exploded in Gangneung City, Gangwondo, South Korea on 23 May 2019. In a chemical facility in Santa Clara, California, a hydrogen storage tank spilt and exploded in June 2019, disrupting the hydrogen supply for local hydrogen fuel cell vehicles. The hydrogen transportation method was involved in the California explosion, which occurred when a hydrogen delivery trailer released high-pressure gaseous hydrogen, causing spontaneous combustion during the leak and discharge, and then a chain explosion. On 4 August 2021, a hydrogen tank in a Shenyang company compound exploded.

Various hydrogen storage technologies have been tried so far, for instance, pressurized gaseous hydrogen storage [2–4], cryogenic liquefaction hydrogen storage [4,5], carbonaceous materials hydrogen storage [4,6–8], metal alloy hydrogen storage [9], complexation hydride hydrogen storage [10,11], glass microspheres hydrogen storage [12], liquid organic

hydrogen storage [13–15], and so on. Although most of them are well-developed, their efficiency is still low. Organic liquid hydrogen storage, for example, is safe and convenient to carry, has considerable hydrogen storage capacity, is recyclable, and uses little energy [16]. However, technological barriers must be overcome, such as sophisticated dehydrogenation technology, high dehydrogenation energy consumption, and off-line catalyst technology. Since the 1980s, reversible hydrogen storage in liquid organic hydrogen carriers (LOHC) has been promoted as a key technology for the energy transition from fossil fuels to renewable energy sources [17–19]. To store hydrogen safely and efficiently for a long time, the carrier compound must have considerable activation energy. The thermal stability of the compound can be improved by adding a catalyst. A safe and suitable compound can improve the efficiency of hydrogen storage.

Wang [20] added three iridium complexes, $IrH_2\{C_6H_32,6(CH_2PBU_2^t)_2\}$, $IrH_2\left\{C_6H_32,6\left(CH_2PBr_2^i\right)_2\right\}$, and $IrHCL\{C_6H_32,6(OPBU_2^t)_2\}$, to N-Ethylcarbazole to improve the dehydrogenation reaction of N-Ethylcarbazole. Studies have shown that $IrHCL\{C_6H_32,6(OPBU_2^t)_2\}$ is the most active catalyst, which not only maintains its activity at 150 °C, but also improves the thermodynamic constraints.

Sotoodeh [21] found that catalysts with different mass ratios of Pd/SiO_2 have good catalytic dehydrogenation activity for perhydro N-Ethylcarbazole (12H-NECZ) at 150–170 °C, and 4.0 wt% Pd/SiO_2 can achieve 100% conversion at 170 °C, whereas H_2 recovery reaches 69%.

Yang et al. [22] compared the catalytic dehydrogenation activities of four commercially supported noble metal catalysts supported by Al_2O_3 for perhydro N-Ethylcarbazole (H12-NEC). The order of performance size was: Pd > Pt > Ru > Rh. Among them, under the experimental conditions, only Pd and Pt could satisfy the conditions of complete dehydrogenation and 100% selectivity to perhydro N-Ethylcarbazole.

Two organic liquid hydrogen storage materials, N-Ethylcarbazole (NE) and Carbazole, were utilized as carriers in this experiment, along with two catalysts, Tin(II) Oxide (SnO) and Lithium oxide (Li_2O). To determine kinetic parameters, kinetic analysis used thermogravimetric (TG) and differential thermogravimetry (DTG) data. This research can be utilized to assess the thermal hazard mechanism of organic liquids, including catalysts, and to reduce industrial accidents when hydrogen is stored and transported, using NE and Carbazole as a reference.

2. Experimental Methods

2.1. Samples

The primary materials involved in the experiment included lithium oxide (CAS number: 12057-24-8), N-Ethylcarbazole (CAS number: 86-28-2), Carbazole (CAS number: 86-74-8), and tin(II) oxide (CAS number: 21651-19-4) and were purchased from Adamas Reagent, Ltd.

Before the experiment, the experimental items used were stored in a dry vacuum to avoid interaction with external conditions.

The structure of liquid organic hydrogen carriers is presented in Figure 1 [23].

2.2. Sample Preparation

This experiment used Thermogravimetric Analysis (TGA2, Mettler-Toledo Co., Zurich, Switzerland) [24–27] and Differential Scanning Calorimetry (HP DSC3, Mettler-Toledo Co., Zurich, Switzerland) equipment [28,29] for testing. TG had to maintain control of the heating rate (β) as well as assess the weight loss. The sample sizes were 10 mg and 0.1 mg, with a mass ratio of 1:9 for lithium oxide and tin oxide to Carbazole and NE. The temperature range for heating was 30–300 °C. In this experiment, the β was set at 1, 2, 4, 6, and 10 °C/min to ensure the highest and minimum β ratios were higher than 5. The same β of 10 was used in the Differential Scanning Calorimetry (DSC) experiment, and the sample quality was the same as in the TG experiment.

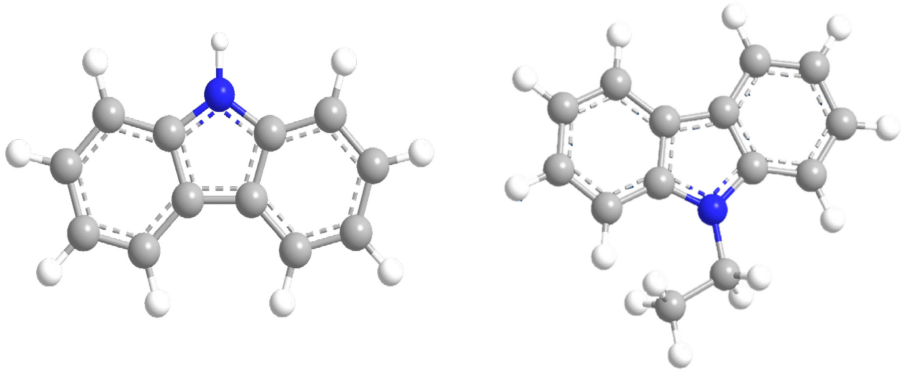

(**a**) (**b**)

Figure 1. The structure of liquid organic hydrogen carriers (LOHC): (**a**) Carbazole; (**b**) N-Ethylcarbazole.

2.3. Catalyst Dehydrogenation Principle

The dehydrogenation reaction in this study is the dehydrogenation reaction of NE and Carbazole at high temperatures and in the presence of catalysts (SnO and Li_2O). Using a suitable catalyst to catalyze the dehydrogenation of the compound, the purpose of dehydrogenation can be achieved, and the carbon–hydrogen bond that can be broken and the carbon–carbon bond that can be damaged must be maintained. The schematic diagram is shown in Figure 2 [23].

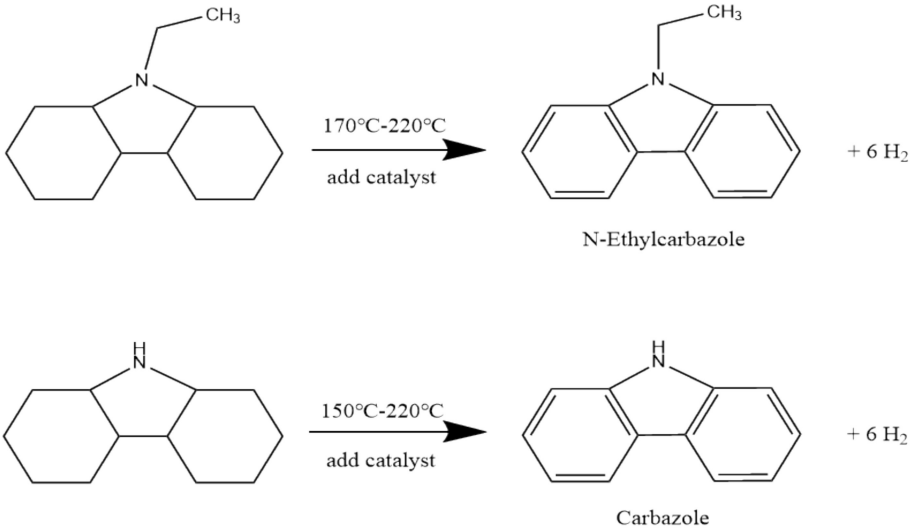

Figure 2. Schematic diagram of dehydrogenation of NE and Carbazole at elevated temperature and in the presence of catalysts (SnO and Li_2O).

2.4. Kinetic Model

2.4.1. FWO Method

The Flynn–Wall–Ozawa method is currently a widely used integration method of thermodynamic analysis [30]. Different values of β are found with the same α, where G(α) is a fixed value, lgβ and $1/T$ are linear relations, and E_a is calculated from the slope. The kinetic equation is presented as the following Equation (1) [24]:

$$\ln \beta = \ln\left(\frac{AE_a}{R \cdot G(\alpha)}\right) - 2.315 - 0.4567\frac{E_a}{R \cdot T} \quad (1)$$

2.4.2. Vyazovkin Method

The Vyazovkin method is a model-free kinetic integration method, which can find the equivalent conversion method of the corresponding temperature function under the same conversion rate α, where $t_{\alpha,t}$ is the time required to reach various conversion rates. Its formula is shown in the following equation [28,31]:

$$-\ln t_{\alpha,\mathrm{t}} = \ln\left[\frac{A_\mathrm{a}}{g(\alpha)}\right] - \frac{E_\mathrm{a}}{R \cdot T_\mathrm{i}} \tag{2}$$

2.4.3. Kissinger Method

The Kissinger equation is based on the Arrhenius equation, which leads to the following equations:

$$\frac{d\alpha}{dt} = k(T)f(\alpha) = A\,exp\left[-\frac{E_\mathrm{a}}{R \cdot T}\right]f(\alpha) \tag{3}$$

when $T = T_\mathrm{p}$, $d^2\alpha/dt^2 = 0$. Substitute into Equation (3) to obtain [28]:

$$\frac{d^2\alpha}{d^2t} = \left[\frac{E_\mathrm{a}\beta}{R \cdot T_\mathrm{P}^2} + Af'(\alpha_\mathrm{m})exp\left(-\frac{E_\mathrm{a}}{R \cdot T_\mathrm{p}}\right)\right]\left(\frac{d\alpha}{dt}\right)_\mathrm{m} = 0 \tag{4}$$

where $f'(\alpha) = df(\alpha)/d\alpha$, and m is the value at the maximum transition. Kissinger assumed that $f'(\alpha_\mathrm{m})$ is independent of β and that $f'(\alpha_\mathrm{m})$ is approximately equal to 1.0. By a simple logarithmic transformation, Equation (4) becomes [28]:

$$\ln\left(\frac{\beta}{T_m^2}\right) = ln\left(-\frac{AR}{E_\mathrm{a}}f'(\alpha_m)\right) - \frac{E_\mathrm{a}}{R \cdot T_m} \tag{5}$$

2.4.4. KAS Method

The Kissinger–Akahira–Sunose (KAS) kinetic model is considered an evaluation of the Arrhenius equation using a differential method, and the Arrhenius model equation is [32]:

$$k = Aexp\left(-\frac{E_\mathrm{a}}{R \cdot T}\right) \tag{6}$$

k has a linear relationship with the reaction temperature [28]. The reaction rate can be converted to the change in the conversion rate per unit time, as shown in Equations (7) and (8) [28].

$$\frac{d\alpha}{dt} = kf(\alpha) \tag{7}$$

$$f(\alpha) = (1-\alpha)^n \tag{8}$$

Combining Equations (6)–(8), they can be rewritten as [33]:

$$\frac{d\alpha}{dt} = Aexp\left(-\frac{E_\mathrm{a}}{R \cdot T}\right)(1-\alpha)^n \tag{9}$$

Then, taking the derivative of Equation (9), Equation (10) can be obtained:

$$\frac{d}{dt}\left[\frac{d\alpha}{dt}\right] = \frac{d\alpha}{dt}\left[\frac{E_a\frac{dT}{dt}}{R \cdot T^2} - An(1-\alpha)^{n-1}exp\left(-\frac{E_\mathrm{a}}{R \cdot T_\mathrm{P}}\right)\right] \tag{10}$$

Since A, $f(\alpha)$, and E_a are all affected by temperature T, E_a and A have nothing to do with α. Therefore, Equation (10) can be extended to Equations (11) and (12) [33]:

$$\frac{E_\mathrm{a}\beta}{R \cdot T_\mathrm{p}^2} = Aexp\left(-\frac{E_\mathrm{a}}{RT_\mathrm{p}}\right) \tag{11}$$

$$\ln\left(\frac{\beta}{T_{\mathrm{p}}^2}\right) = ln\left(\frac{A}{E_{\mathrm{a}}g(\alpha)}\right) - \frac{E_{\mathrm{a}}}{R \cdot T_{\mathrm{P}}} \tag{12}$$

2.4.5. Starink Method

To obtain better thermodynamic parameters, the KAS equation is slightly adjusted by the Starink model, and Equation (13) can be obtained after adjustment [28]:

$$\ln\left(\frac{\beta}{T^{\mathrm{i}}}\right) = C_{\mathrm{s}} - C\left(\frac{E_{\mathrm{a}}}{R \cdot T}\right) \tag{13}$$

where i and C are approximated values using a specific type of integrated temperature. C_{s} is usually constant. According to the KAS kinetic model, when E_{a} is i = 1.8 and C = 1.0037, the calculation of E_{a} is more accurate, and Equation (14) is as follows [28]:

$$\ln\left(\frac{\beta}{T^{1.8}}\right) = C_s - 1.0037\left(\frac{E_{\mathrm{a}}}{R \cdot T}\right) \tag{14}$$

3. Results

3.1. DSC Analysis

Figure 3 shows the DSC results of the heat flow as a function of temperature for pure Carbazole and Carbazole, plus two catalysts with 10% mass SnO and Li_2O, respectively. Carbazole and NE are both crystalline at standard temperature and pressure, so when Carbazole and NE reach the melting point, the melting endotherm produces the first endothermic peak, and the second endothermic peak is the temperature at which Carbazole and NE dehydrogenate. Pure Carbazole was used as the reference group: the initial temperature T_0 was 310.94 °C, the peak temperature was 334.34 °C, the maximum heat release rate was 2.072 mW/mg, and the total released heat was 243.75 J/g. The T_0 of Carbazole plus SnO and Li_2O were 348.67 and 347.48 °C, respectively; the peak temperatures were 354.54 and 354.76 °C; the maximum heat release rates were 4.22 and 4.71 mW/mg, respectively, at 253.10 and 262.38 J/g. Pure NE was used as the reference group: the initial temperature T_0 was 342.01 °C, the peak temperature was 344.43 °C, the maximum heat release rate was 7.45 mW/mg, and the total released heat was 277.69 J/g. The T_0 of NE plus SnO and Li_2O were 339.98 and 331.98 °C, respectively, the peak temperatures T_{p} were 341.89 and 342.41 °C, and the maximum heat release rates were 5.98 and 2.64 mW/mg, respectively. The total released heat was 189.46 and 191.92 J/g, respectively.

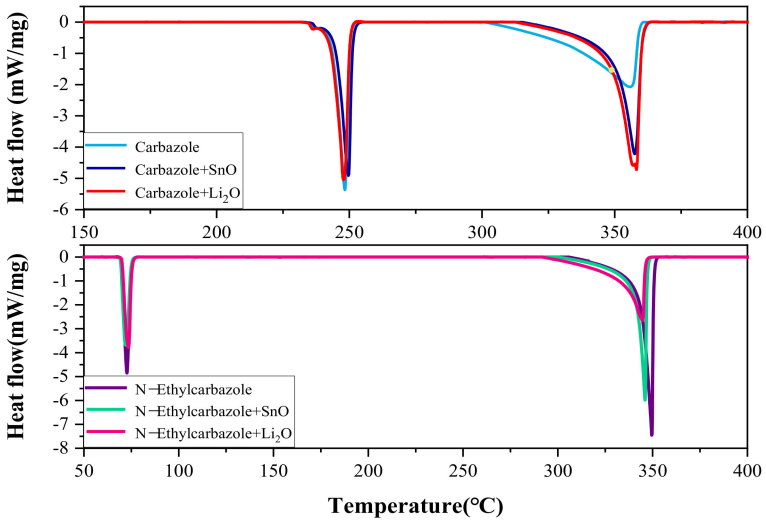

Figure 3. Heat fluxes versus temperatrue of Carbazole, NE, and mixtures.

The DSC results show that mixing NE with two catalysts of SnO and Li_2O can advance the onset temperature of dehydrogenation, reduce the maximum heat release rate and total heat release rate of the mixture, and reduce the maximum heat release rate and the thermal hazard of NE.

3.2. Thermogravimetric Analysis

Figure 4 displays the TG and DTG curves of mass loss and mass loss derivative versus temperature for Carbazole and NE with added Li_2O and SnO, separately.

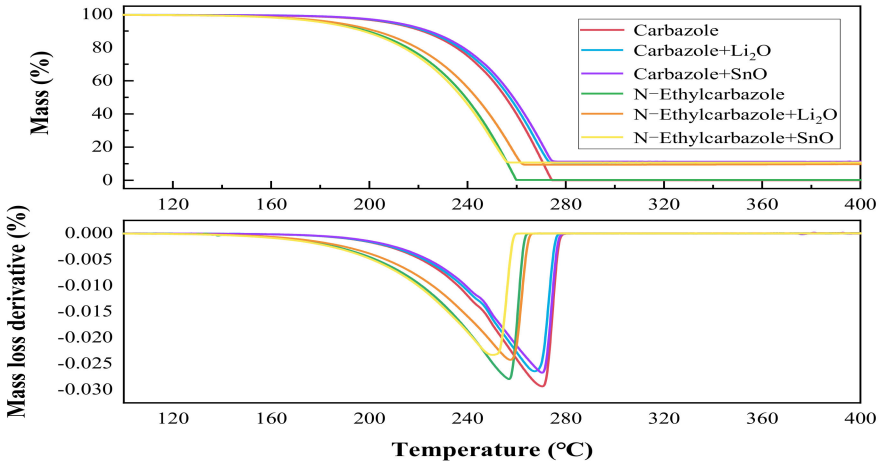

Figure 4. Mass loss and mass loss derivative versus temperature of TG-DTG curves for Carbazole and N-Ethylcarbazole and with additives.

The results showed that the maximum temperature of mass loss of pure Carbazole and pure NE were 273.62 and 258.33 °C, and the mass loss rates were −0.02933 and −0.02794 per/min, respectively. The maximum temperature of mass loss of Carbazole + Li_2O and Carbazole + SnO were 269.91 and 272.30 °C. This shows that when the release of hydrogen reaches the maximum, the mass loss rates were −0.02642 per/min and −0.02671 per/min, respectively. The maximum temperature of mass loss of NE + Li_2O and NE + SnO were 262.5 and 250.7 °C, and the mass loss rates were −0.02423 and −0.02328 per/min, respectively. The maximum temperature and mass loss rate of pure Carbazole and pure NE were lower than of Carbazole + Li_2O, Carbazole + SnO, NE + Li_2O, and NE + SnO. The results indicated that Li_2O and SnO significantly increased the dehydrogenation yields of Carbazole and NE. They showed that the onset temperature of dehydrogenation of NE (154.16 °C) was lower than that of Carbazole (175.33 °C), and the onset temperature of dehydrogenation of the mixture of NE and SnO (141.50 °C) was lower than that of pure NE and hydrogen emissions. As the temperature increased, the hydrogen release rate was faster, so that SnO had a lower effect on reducing NE. Therefore, the onset temperature of the dehydrogenation of the Carbazole was promoted. After adding a catalyst, the dehydrogenation yield increased, but the dehydrogenation temperature increased relatively, and different catalysts had different E_a.

Figure 5 illustrates the thermal weight loss rate of NE mixed with SnO: the higher the β, the longer the dehydrogenation initiation time is delayed. For example, when the β is 10 °C/min, the starting temperature of dehydrogenation is about 190 °C, and the end temperature is about 260 °C. When the β is 1 °C/min, the dehydrogenation starts at 130 °C and ends at 200 °C, and the dehydrogenation reaction achieves effective dehydrogenation at low temperature. At the same time, the DTG diagram shows that the dehydrogenation rate gradually slows down with the increase in the β.

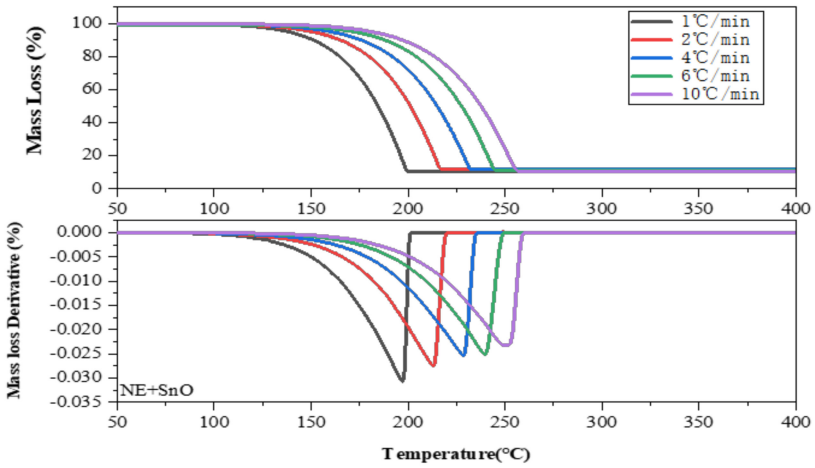

Figure 5. Curve of thermogravimetric loss of NE + SnO at β of 1.0, 2.0, 4.0, 6.0, and 10.0 °C/min in TG experiments.

3.3. Kinetic Results

Different catalysts used in various organic liquid hydrogen storage materials will increase the dehydrogenation yield, but relatively speaking, the dehydrogenation temperature will increase, and multiple catalysts have different activation energies.

Since NE has a lower dehydrogenation temperature and a lower heat release rate than Carbazole, and NE plus SnO has the lowest dehydrogenation temperature and a lower heat release rate, a detailed thermodynamic analysis was carried out for its activation thermokinetic parameters.

We determined the thermokinetic parameters based on the TG experiment. Figure 6a illustrates the linear fitting results of $\ln\left(\beta/T_p^2\right)$ versus $1/T$ for NE + SnO: the slope of the fitting line is -9550.87, the coefficient of determination R^2 is 0.99751, and E_a is 79.40 kJ, according to the equation/mol.

To confirm the reliability of our data, we continued to analyze the experimental data using a variety of isotransformation methods, and multiple comparisons yielded reliable data.

We also used FWO, Vyazovkin, Starink, and KAS, four methods to verify the reliability of our data, and 12 different α of five β were selected for the differential. Figure 6b shows the fitting results using the Vyazovkin method under different α, and the consequences of FWO, KAS, and Starink are shown in Figure 6c–e, respectively.

Figure 6b–e illustrate the linear relationship between 12 conversion rates α using five heating rates β in four different models. The trends are similar: E_a and R^2 gradually increase with the increase in α, and the linear functions obtained by the KAS method and the Starink method are almost the same. To further prove the accuracy of the data, E_a and R^2 of the four methods are set out in Table 1 for further details. Table 1 lists the thermodynamic models of FWO, KAS, Starink and Vyazovkin, and the E_a and R^2 of NE + SnO were summarized and averaged. The results were only slightly different, with R^2 reaching 0.995, close to 1, proving that our experimental data were reliable: the mean E_a of NE + SnO is 74.1291 kJ/mol.

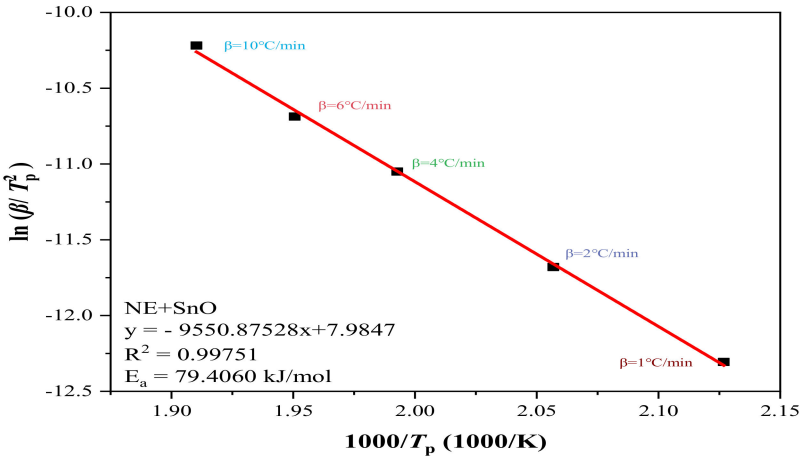

(**a**)

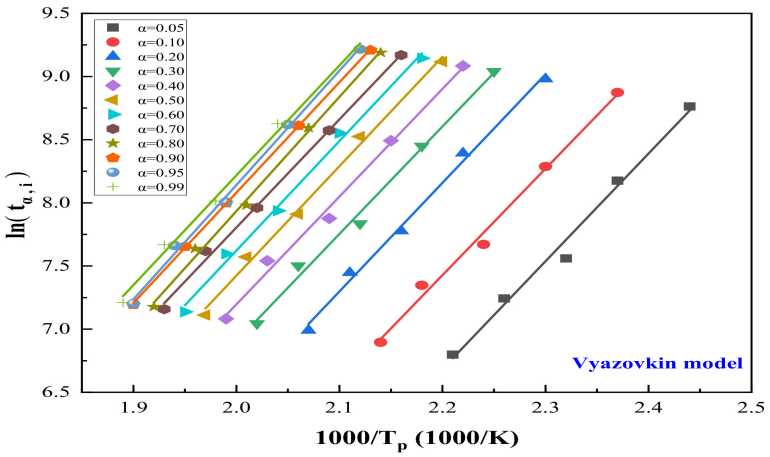

(**b**)

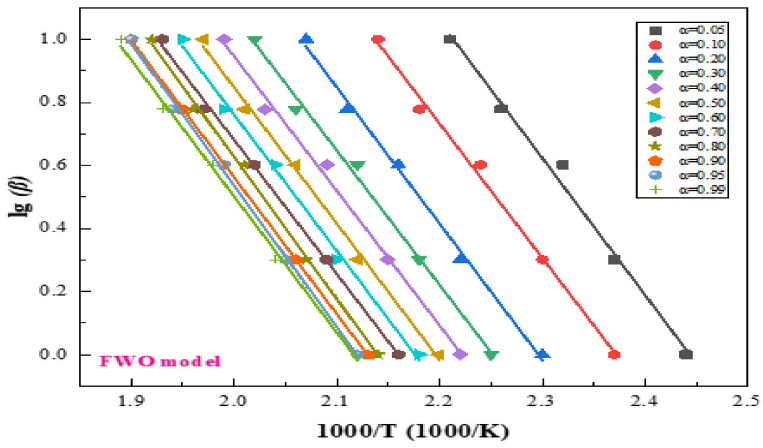

(**c**)

Figure 6. *Cont.*

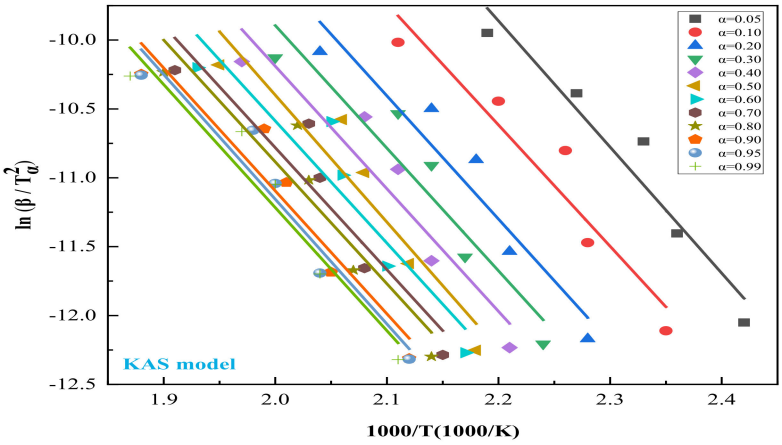

(**d**)

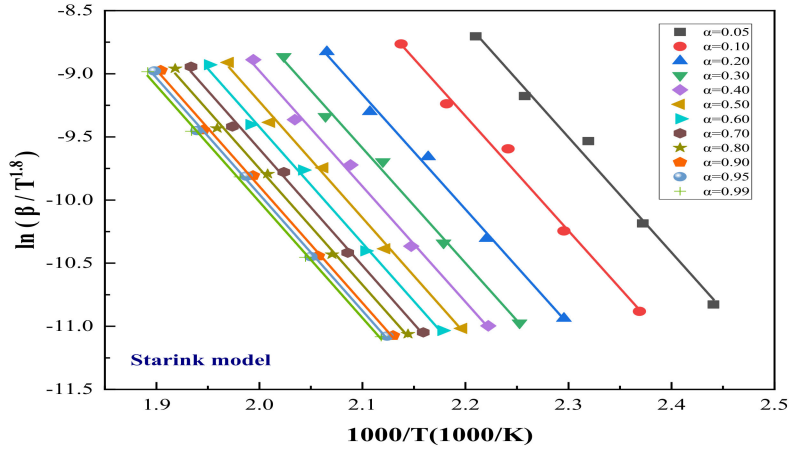

(**e**)

Figure 6. Diagram of NE + SnO in TG experiments through four kinetic simulation methods: (**a**) E_a determination from Kissinger method of various β; (**b**) differential isoconversional analysis of using Vyazovkin method at β of 1, 2, 4, 6, and 10 °C/min; (**c**) differential isoconversional analysis of using FWO method at β of 1, 2, 4, 6, and 10 °C/min; (**d**) differential isoconversional analysis of using KAS method with β of 1, 2, 4, 6 and 10 °C/min; (**e**) differential isoconversional analysis of using Starink method at β of 1, 2, 4, 6, and 10 °C/min.

Table 1. Calculated E_a and R^2 values through FWO, KAS, Starink, and Vyazovkin methods.

α	E_a (kJ/mol)				R^2			
	FWO	**KAS**	**Starink**	**Vyazovkin**	**FWO**	**KAS**	**Starink**	**Vyazovkin**
0.05	76.5694	73.5177	73.9443	68.6312	0.9916	0.9898	0.9900	0.9889
0.10	76.5521	73.2751	73.7249	69.0830	0.9939	0.9925	0.9927	0.9918
0.20	76.8145	73.3111	73.7847	69.7472	0.9954	0.9944	0.9945	0.9939
0.30	76.9816	73.3385	73.8268	70.1174	0.9960	0.9951	0.9952	0.9946
0.40	77.3591	73.6275	74.1255	70.6376	0.9962	0.9954	0.9955	0.9949
0.50	77.9042	74.1113	74.6164	71.3031	0.9968	0.9962	0.9963	0.9958
0.60	77.9449	74.0790	74.5918	71.4166	0.9970	0.9964	0.9965	0.9960
0.70	78.1922	74.2717	74.7904	71.7359	0.9974	0.9969	0.9970	0.9966
0.80	78.0924	74.1078	74.6330	71.6789	0.9977	0.9973	0.9973	0.9969
0.90	78.2789	74.2472	74.7775	71.9188	0.9980	0.9976	0.9976	0.9973
0.95	78.2633	74.2073	74.7401	71.9196	0.9979	0.9975	0.9975	0.9971
0.99	78.0864	73.9968	74.5328	71.7510	0.9984	0.9981	0.9981	0.9978
Average	77.5866	73.8409	74.3407	70.8284	0.9964	0.9956	0.9957	0.9957

Table 2 shows that the E_a of Carbazole after adding the catalyst is always higher than that of the NE mixed catalyst, and the Li_2O catalyst makes the E_a of Carbazole the highest, up to 108.98 kJ/mol.

Table 2. Calculated $\overline{E_a}$ and R^2 values from NE and Carbazole mixed with catalysts.

Material	Methods										Average
	FWO		Kissinger		Starink		KAS		Vyazovkin		
	$\overline{E_a}$	R^2	$\overline{E_a}$	R^2	$\overline{E_a}$	R^2	$\overline{E_a}$	R^2	$\overline{E_a}$	R^2	$\overline{E_a}$
NE + SnO	77.5866	0.9964	79.4059	0.9975	74.3407	0.9957	73.8409	0.9956	70.8284	0.9951	75.2005
NE + Li_2O	76.8964	0.9196	73.5065	0.8202	73.5426	0.9043	73.0315	0.9024	70.1894	0.8971	73.4332
Carb + SnO	102.0030	0.9981	96.0449	0.9900	99.5507	0.9979	99.1028	0.9978	96.9057	0.9977	98.7214
Carb + Li_2O	109.4175	0.9971	112.3608	0.9986	107.3061	0.9967	106.8855	0.9966	104.7156	0.9966	108.1371

The Li_2O catalyst enhances the activation energy of Carbazole, and the SnO catalyst is more effective in enhancing the activation energy of NE.

4. Discussion

In the past, experiments have proved the feasibility of NE and Carbazole as organic liquid hydrogen storage materials. For example, the dehydrogenation temperature is low, and their safety is relatively low. The addition of metal oxide dehydrogenation catalysts to organic liquid hydrogen storage materials has been under investigation to reduce their dehydrogenation temperature and improve their thermal stability, but few thermodynamic analyses and comparative experiments have been conducted.

We performed DSC and TG calorimetry experiments and analyzed and compared the results of various linear regression methods. The DSC results show that the metal oxide has a significant delaying effect on the occurrence time of the initial thermal reaction and reduces its endothermic heat. The addition of SnO to reduce the endothermic heat of NE echoes the increase in E_a obtained from the TG experimental results. Furthermore, the addition of NE to SnO would be safer than Li_2O.

We added the two metal oxides Li_2O and SnO to Carbazole and NE and used five thermodynamic methods. After simulation with different β and α, we found that adding additives can improve the safety of hydrogen storage materials and increase the dehydrogenation temperature. This study provides a scientific basis for adding metal oxidants to NE and Carbazole. More research is still required to find suitable additives for organic liquid hydrogen storage materials.

5. Conclusions

The addition of metal oxide dehydrogenation catalysts to organic liquid hydrogen storage materials has been investigated to reduce their dehydrogenation temperature and improve thermal stability. In this study, the thermal analysis and kinetic analysis of pure Carbazole and pure NE and the mixture of two catalysts, SnO and Li_2O, respectively, revealed that the addition of catalysts could improve the performance of Carbazole and NE. It provides a reference for studying the thermal stability of organic liquid hydrogen storage materials after adding catalysts. From the paper, the following conclusions can be drawn:

(1) Different metal oxidation catalysts affect the dehydrogenation temperature of different organic liquid hydrogen storage materials. For example, of the two organic liquid hydrogen storage materials, the dehydrogenation temperature of Carbazole is higher than that of NE. On the other hand, the dehydrogenation temperature of NE + SnO is 258.33 °C, lower than that of pure NE, at 250.7 °C. The addition of SnO provides high-efficiency low-temperature dehydrogenation, indicating that SnO is an ideal dehydrogenation catalyst for NE.

(2) Through thermokinetic analysis, E_a generally increases after adding a catalyst, proving that NE and Carbazole will be more stable after adding SnO and Li_2O. SnO has a

good effect on the activation energy of NE, with E_a at 76.29 kJ/mol. Li_2O has a good effect on the activation energy of Carbazole, with E_a at 108.98 kJ/mol. The calculated activation energy of Carbozole is generally higher than that of NE, which corresponds to the higher dehydrogenation temperature of Carbazole than that of NE in the TGA experiment.

(3) This study provides feasible experimental data for further research on adding metal oxides to organic liquid hydrogen storage materials. Based on the two metal oxide catalysts discussed in this study, the feasibility of adding SnO to NE has been demonstrated. This research is attractive and promising from the perspective of experimental data and application. The selection of suitable catalysts for organic hydrogen storage materials will remain the focus of future research.

Author Contributions: Writing—review and editing, L.-J.X. and A.-C.H.; Formal analysis, A.-C.H.; data curation: Y.-C.L.; Conceptualization, Y.T.; Methodology, H.-L.Z.; Supervision, Z.-X.X.; funding acquisition, J.-C.J. All authors have read and agreed to the published version of the manuscript.

Funding: This research was funded by National Natural Science Foundation of China (No. 21927815) and the National Key Research Development Program of China (Nos. 2019YFC0810701 and 2021YFC3001203).

Institutional Review Board Statement: Not applicable.

Informed Consent Statement: Not applicable.

Conflicts of Interest: The authors declare no conflict of interest.

Nomenclature

Roman Symbols

Symbol	Unit	Description
ΔH_d	J/g	Heat of decomposition
A	1/s	Frequency factor
C	dimensionless	Constant
C_s	dimensionless	Constant for Starink method
E_a	kJ/mol	Apparent activation energy
f(α)	dimensionless	Differential form of reaction mechanism function
g(α)	dimensionless	Integral kinetic function
n	dimensionless	Partial order of reaction
k		Rate constant at infinite temperature
K	1/min	Reaction rate constant
t	min	Time
T	K	Absolute temperature
T_0	°C	Apparent onset temperature
T_p	°C	Peak temperature
R	8.314J/(mol×K)	Universal gas constant
R^2	dimensionless	Coefficient of determination
Greek Letters		
α	Dimensionless	Conversion degree
β	°C/min	Heating rate
γ	dα/dt	Degree of conversion rate
ρ_s	kg/m^3	Density

Sub- and Superscript

Symbol	Description
LOHC	liquid organic hydrogen carriers
NE	N-Ethylcarbazole
DSC	Differential Scanning Calorimetry
TG	Thermogravimetric
DTG	Differential thermogravimetry

References

1. Schlapbach, L. Hydrogen-storage materials for mobile applications. *Nature* **2001**, *414*, 353–358. [CrossRef] [PubMed]
2. Züttel, A. Materials for hydrogen storage. *Mater. Today* **2003**, *23*, 24–33. [CrossRef]
3. Zheng, J.; Liu, X.; Xu, P.; Liu, P.; Zhao, Y.; Yang, J. Development of high pressure gaseous hydrogen storage technologies. *Int. J. Hydrogen Energy* **2012**, *37*, 1048–1057. [CrossRef]
4. Jiang, Z.; Pan, Q.; Xu, J.; Fang, T. Current situation and prospect of hydrogen storage technology with new organic liquid. *Int. J. Hydrogen Energy* **2014**, *39*, 17442–17451. [CrossRef]
5. Peschka, W.; Carpetis, C. Cryogenic hydrogen storage and refueling for automobiles. *Int. J. Hydrogen Energy* **1980**, 619–626. [CrossRef]
6. Dillon, A.C.; Jones, K.M.; Bekkedahl, T.A.; Kiang, C.H.; Bethune, D.S.; Heben, M.J. Storage of hydrogen in single-walled carbon nanotubes. *Nature* **1997**, *386*, 377–380. [CrossRef]
7. Cheng, H.M.; Yang, Q.H.; Liu, C. Hydrogen storage in carbon nanotubes. *Carbon* **2001**, *39*, 1447–1455. [CrossRef]
8. Mohan, M.; Sharma, V.K.; Kumar, E.A.; Gayathri, V. Hydrogen storage in carbon materials—A review. *Energy Storage* **2019**, *1*, e35. [CrossRef]
9. Cummings, D.L.; Powers, G.J. The Storage of Hydrogen as Metal Hydrides. *Ind. Eng. Chem. Process Des. Dev.* **1974**, *13*, 182–192. [CrossRef]
10. Schuth, F.; Bogdanovic, B.; Felderhoff, M. Light metal hydrides and complex hydrides for hydrogen storage. *Chem. Commun.* **2004**, *2004*, 2249–2258. [CrossRef]
11. Rönnebro, E. Development of group II borohydrides as hydrogen storage materials. *Curr. Opin. Solid State Mater. Sci.* **2011**, *15*, 44–51. [CrossRef]
12. Schmitt, M.L.; Shelby, J.E.; Hall, M.M. Preparation of hollow glass microspheres from sol–gel derived glass for application in hydrogen gas storage. *J. Non Cryst. Solids* **2006**, *352*, 626–631. [CrossRef]
13. Boudjahem, A.G.; Bouderbala, W.; Bettahar, M. Benzene hydrogenation over Ni–Cu/SiO_2 catalysts prepared by aqueous hydrazine reduction. *Fuel Process. Technol.* **2011**, *92*, 500–506. [CrossRef]
14. Wang, W.T.; Liu, H.Z.; Wu, T.B.; Zhang, P.; Ding, G.D.; Liang, S.G.; Jiang, T.; Han, B.X. Ru catalyst supported on bentonite for partial hydrogenation of benzene to cyclohexene. *J. Mol. Catal. A Chem.* **2012**, *355*, 174–179. [CrossRef]
15. Zieliński, M.; Wojciechowska, M. Iridium supported on MgF_2–MgO as catalyst for toluene hydrogenation. *Catal. Commun.* **2012**, *18*, 1–4. [CrossRef]
16. Deyko, G.S.; Glukhov, L.M.; Kustov, L.M. Hydrogen storage in organosilicon ionic liquids. *Int. J. Hydrogen Energy* **2020**, *45*, 33807–33817. [CrossRef]
17. Newson, E.; Haueter, T.; VonRoth, P.H.F.; Scherer, G.W.H.; Schucan, T.H. Seasonal storage of hydrogen in stationary systems with liquid organic hydrieds. *Int. J. Hydrogen Energy* **1998**, *23*, 905–909. [CrossRef]
18. Teichmann, D.; Arlt, W.; Wasserscheid, P.; Freymann, R. A future energy supply based on Liquid Organic Hydrogen Carriers (LOHC). *Energy Environ. Sci.* **2011**, *4*, 2767–2773. [CrossRef]
19. Niermann, M.; Drünert, S.; Kaltschmitt, M.; Bonhoff, K. Liquid organic hydrogen carriers (LOHCs) – techno-economic analysis of LOHCs in a defined process chain. *Energy Environ. Sci.* **2019**, *12*, 290–307. [CrossRef]
20. Wang, Z.; Tonks, I.; Belli, J.; Jensen, C.M. Dehydrogenation of N-ethyl perhydrocarbazole catalyzed by PCP pincer iridium complexes: Evaluation of a homogenous hydrogen storage system. *J. Organomet. Chem.* **2009**, *694*, 2854–2857. [CrossRef]
21. Sotoodeh, F.; Zhao, L.; Smith, K.J. Kinetics of H_2 recovery from dodecahydro-N-ethylcarbazole over a supported Pd catalyst. *Appl. Catal. A-Gen.* **2009**, *362*, 155–162. [CrossRef]
22. Yang, M.; Dong, Y.; Fei, S.; Ke, H.; Cheng, H. A comparative study of catalytic dehydrogenation of perhydro-N-ethylcarbazole over noble metal catalysts. *Int. J. Hydrogen Energy* **2014**, *39*, 18976–18983. [CrossRef]
23. Heublein, N.; Stelzner, M.; Sattelmayer, T. Hydrogen storage using liquid organic carriers: Equilibrium simulation and dehydrogenation reactor design. *Int. J. Hydrogen Energy* **2020**, *45*, 24902–24916. [CrossRef]
24. Zhou, H.L.; Jiang, J.C.; Huang, A.C.; Tang, Y.; Zhang, Y.; Huang, C.F.; Liu, S.H.; Shu, C.M. Calorimetric evaluation of thermal stability and runaway hazard based on thermokinetic parameters of O,O–dimethyl phosphoramidothioate. *J. Loss Prev. Process Ind.* **2022**, *75*, 104697. [CrossRef]
25. Tsai, Y.T.; Yang, Y.; Huang, H.C.; Shu, C.M. Inhibitory effects of three chemical dust suppressants on nitrocellulose dust cloud explosion. *AIChE J.* **2020**, *66*, e16888. [CrossRef]
26. Gao, X.; Jiang, L.; Xu, Q. Experimental and theoretical study on thermal kinetics and reactive mechanism of nitrocellulose pyrolysis by traditional multi kinetics and modeling reconstruction. *J. Hazard. Mater.* **2020**, 386. [CrossRef] [PubMed]
27. Guo, Y.; Zhao, N.N.; Zhang, T.; Gong, H.; Ma, H.; An, T.; Zhao, F.; Hu, R. Compatibility and thermal decomposition mechanism of nitrocellulose/Cr_2O_3 nanoparticles studied using DSC and TG-FTIR. *RSC Adv.* **2019**, *9*, 3927–3937. [CrossRef]
28. Liu, Y.C.; Huang, A.C.; Tang, Y.; Ma, X.M.; Yang, Y.P.; Wu, Z.H.; Shu, C.M.; Xing, Z.X.; Jiang, J.C. Thermokinetic model establishment and numerical simulation of 2,4,6-trinitrophenol based on eco-friendly synthesis method. *J. Energetic Mater.* **2021**, 1–20. [CrossRef]
29. Liu, S.H.; Hou, H.Y.; Chen, J.W.; Weng, S.Y.; Lin, Y.C.; Shu, C.M. Effects of thermal runaway hazard for three organic peroxides conducted by acids and alkalines with DSC, VSP2, and TAM III. *Thermochim. Acta* **2013**, *566*, 226–232. [CrossRef]

30. Huang, A.C.; Chuang, Y.K.; Huang, C.F.; Shu, C.M. Thermokinetic analysis of the stability of malic and salicylic acids in cosmeceutical formulations containing metal oxides. *J. Therm. Anal. Calorim.* **2017**, *132*, 165–172. [CrossRef]
31. Vyazovkin, S.; Sbirrazzuoli, N. Isoconversional Kinetic Analysis of Thermally Stimulated Processes in Polymers. *Macromol. Rapid Commun.* **2006**, *27*, 1515–1532. [CrossRef]
32. Wang, Q.; Liu, S.H.; Huang, A.C.; Huang, C.F.; Chuang, Y.K.; Shu, C.M. Effects of mixing malic acid and salicylic acid with metal oxides in medium- to low-temperature isothermal conditions, as determined using the thermal activity monitor IV. *J. Therm. Anal. Calorim.* **2018**, *133*, 779–784. [CrossRef]
33. Yang, Y.P.; Huang, A.C.; Tang, Y.; Liu, Y.C.; Wu, Z.H.; Zhou, H.L.; Li, Z.P.; Shu, C.M.; Jiang, J.C.; Xing, Z.X. Thermal Stability Analysis of Lithium-Ion Battery Electrolytes Based on Lithium Bis(trifluoromethanesulfonyl)imide-Lithium Difluoro(oxalato)Borate Dual-Salt. *Polymers* **2021**, *13*, 707. [CrossRef]